Differential Mass and Energy Balances in the Flame Zone From a Practical Fuel Injector in a Technology Combustor

D. L. Warren
Mechanical Engineering Department.

P. O. Hedman
Chemical Engineering Department.

Advanced Combustion Engineering Research Center,
Brigham Young University,
Provo, UT 80642

This paper presents further analysis of experimental results from an Air Force program conducted by researchers at Brigham Young University (BYU), Wright-Patterson Air Force Base (WPAFB), and Pratt and Whitney Aircraft Co. (P&W) (Hedman et al., 1994a, 1995). These earlier investigations of the combustion of propane in a practical burner installed in a technology combustor used: (1) digitized images from video and still film photographs to document observed flame behavior as fuel equivalence ratio was varied, (2) sets of LDA data to quantify the velocity flow fields existing in the burner, (3) CARS measurements of gas temperature to determine the temperature field in the combustion zone, and to evaluate the magnitude of peak temperature, and (4) two-dimensional PLIF images of OH radical concentrations to document the instantaneous location of the flame reaction zones. This study has used the in situ velocity and temperature measurements from the earlier study, suitably interpolated, to determine local mass and energy balances on differential volume elements throughout the flame zone. The differential mass balance was generally within about ±10 percent with some notable exceptions near regions of very high shear and mixing. The local differential energy balance has qualitatively identified the regions of the flame where the major heat release is occurring, and has provided quantitative values on the rate of energy release (up to -400 kJ/m^3 s). The velocity field data have also been used to determine Lagrangian pathlines through the flame zone. The local velocity and temperature along selected pathlines have allowed temperature timelines to be determined. The temperature generally achieves its peak value, often near the adiabatic flame temperature, within about 10 ms. These temperature timelines, along with the quantitative heat release data, may provide a basis for evaluating kinetic combustion models.

Introduction

As part of an earlier study, a practical fuel injector was used in a technology combustor to investigate flame behavior in a jet engine combustor (Hedman et al., 1994, 1995). This earlier study investigated the combustion of gaseous propane with a practical injector installed in a technology combustor that simulates the flow and geometric characteristics of a real jet engine (Sturgess et al., 1992). The technology combustor with the practical high swirl injector is referred to in this paper as the Task 150-HS combustor. These previously reported experimental results were obtained from identical technology combustors located at both BYU and WPAFB. This earlier study was conducted as part of an ongoing investigation into the combustion characteristics of jet engine combustors that has been conducted by the Aero Propulsion and Power Laboratory at Wright Patterson Air Force Base, Pratt and Whitney Aircraft, Inc., and Brigham Young University.

The earlier study used: (1) digitized film and video images to document flame behavior as fuel equivalence ratio was varied, (2) sets of LDA data to quantify the velocity flow fields existing in the burner, (3) CARS measurements of gas temperature to determine the temperature field in the combustion zone, and to evaluate the magnitude of peak temperature, and (4) two-dimensional PLIF images of OH radical concentrations to document the instantaneous location of the flame reaction zones.

The LDA measurements presented previously (Hedman et al., 1994, 1995) have quantified the axial, radial, and tangential velocity components in the combustor for two operating conditions (ϕ = 0.72 and ϕ = 1.49) at an air flow rate of 500 slpm. This information has yielded local mean axial and radial velocity data in the flame zone. CARS gas temperature data were also collected for the Task 150-HS technology at an air flow rate of 500 slpm and at fuel equivalence ratios (ϕ) of 0.75, 1.00, 1.25, and 1.50.

The appropriately interpolated mean gas temperatures for ϕ = 0.75 and 1.50, along with the companion set of gas velocity data, have been used to determine the local mass balance on differential volumes through the flame zone, to determine a local differential energy balance (local energy release rate), Lagrangian pathlines, and temperature time lines through selected regions of the flame. This additional analysis of the measured mean flow and temperature properties was conducted in an attempt to gain additional insights about the combustion processes, and to provide some rate data that might be useful in the evaluation of kinetic models of the combustion processes.

Combustor Test Facility

The Task 150-HS combustor utilized in this study was a modification of a burner designed to investigate lean blowout in the combustors of aircraft gas turbine engines (Sturgess et al., 1992). The Task 150-HS burner, shown schematically in Fig. 1, uses a practical liquid fuel injector with air blast atomi-

Contributed by the International Gas Turbine Institute and presented at the 40th International Gas Turbine and Aeroengine Congress and Exhibition, Houston, Texas, June 5–8, 1995. Manuscript received by the International Gas Turbine Institute February 10, 1995. Paper No. 95-GT-112. Associate Technical Editor: C. J. Russo.

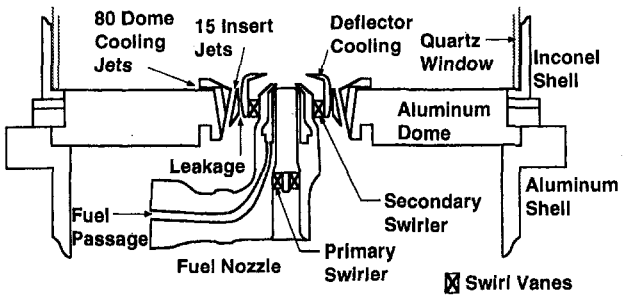

Fig. 1 Schematic of the T150-HS injector

zation, involving coswirling airsheets on either side of a coswirling annular (normally liquid) fuel sheet. The outer air passage and the fuel passage both converge on the central air passage. For this study, the burner was fueled by gaseous propane. Only data from a high-swirl configuration are reported in this paper.

The geometry of the technology combustor is shown schematically in Fig. 2. The cross section of the combustion chamber is square with filleted corners to minimize secondary flow development. The hydraulic diameter is 150 mm. This box-section combustor with corner fillets allows reasonable optical access while providing a cross section that approximates a two-dimensional axisymmetric cross section. The bluff body provides a recirculation region, which can stabilize the flame. Optical windows of fused quartz, about 60 mm in width and 490 mm in length, are provided on the four flat sides to allow laser-based optical diagnostic instruments to be used. Exit blockage of 45 percent is achieved by means of an orifice plate. The only air addition in this configuration is through the dome. This configuration allows measurements to be made in a geometry that embodies features of an actual jet engine combustor, but in a near axisymmetric configuration that is easier to model mathematically.

The combustor is mounted on a 240-mm-long spool piece containing a mounting pad for the fuel injector flange. The combustor and spool piece are situated on an inlet air conditioning section, also shown in Fig. 2. Reactants are supplied at ambient temperature and pressure. Ignition is by means of a removable torch-ignitor.

In an actual engine combustor, additional combustion and cooling air is added to the combustor downstream of the actual fuel injector. This adds an additional complexity to the flow and combustion characteristics, which has not been a part of this investigation. Only the analyses of the flame zone near the injector are presented in this paper.

The work reported herein was accomplished in identical combustors available in the Combustion Laboratories at BYU and WPAFB, respectively. The combustors were designed by researchers at P&W (Sturgess et al., 1992) and fabricated at WPAFB. The high-swirl (HS) injector has a nominal swirl number (based on vane angle) of 1.41, a total air passage effective area of 0.176 in.^{2}, and outer to inner flow splits of 2.8. The outer swirler vane angle was 55 deg. The inner swirler vane angle was 70 deg. The injector was mounted in a plain bulkhead dome containing insert jets angled at 12.5 deg into the flame, and radially outward flowing film cooling jets. This arrangement closely simulates that of an engine combustor. The total effective air flow area of the dome, excluding the fuel injector, was 0.160 in^2.

In order to separate the effects of liquid fuel atomization and spray droplet evaporation from the effects associated with fuel/air mixing and aerodynamic flow pattern, the results reported in this paper were for experiments using only a gaseous propane fuel.

Photographic Flame Characterization

The structure of the flame zone with the Task 150-HS burner was found to be strongly dependent on the fuel equivalence ratio (Hedman et al., 1994). The flame attaches to the burner or lifts from the burner as the fuel equivalence ratio (ϕ) is changed. Each flame shape indicates a different mode of operation, which differ from one another in the location of the flame fronts, or by some structure such as thickness or intensity. The different structures observed arise from changes in the flow fields, mixing patterns, or fuel equivalence ratio as operating conditions are varied.

Isochromatic contours from digitized and filtered video images have been used to record the flame shapes observed visually. Example images at ϕ = 0.75, 1.00, 1.25, and 1.50 are presented in Fig. 3 to provide the reader an indication of the variation in flame structure as ϕ is changed from fuel-lean to fuel-rich operation. The fuel equivalence ratios where the flame transitions from one flame structure to another were determined as a function of fuel flow rate. The flames for both Task 150 injectors were attached to the outside of the insert air jets when the burner was operated very fuel-rich. The flame would then lift, reattach, and lift again as the fuel equivalence ratio was progressively reduced depending on the injector (high swirl versus low swirl) and the air flow rate. During the reattachment phase, the flame would take on many of the characteristics of a strong vortex.

The observed characteristics of the flame as the fuel equivalence ratio was varied were discussed previously (Hedman et al., 1994). However, there are two structures that are of particular interest to this study, those at ϕ = 0.75 and ϕ = 1.50. At ϕ = 0.75, the flame was strongly attached to the center of the burner. At ϕ = 1.50, the flame was lifted, and seemed to be attached to the supplemental air entering the burner through the insert jets. Evaluation of the local stoichiometry from an air flow partitioning analysis showed that in this fuel-rich case, the local fuel equivalence ratio directly over the injector was in excess of the rich flammability limit (Hedman et al., 1994).

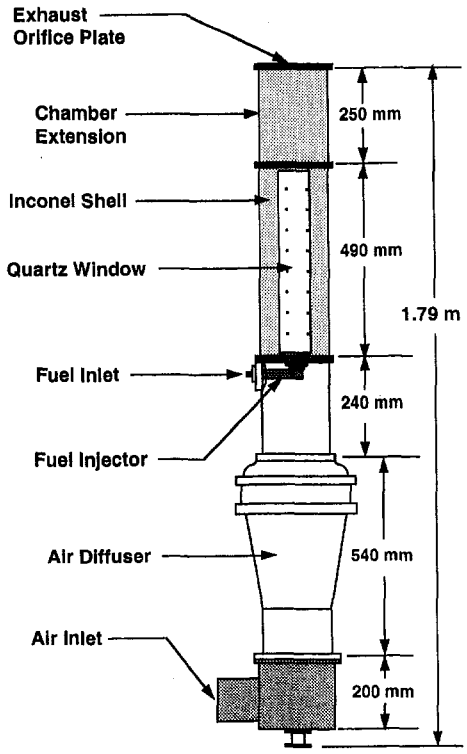

Fig. 2 Laboratory-scale gas turbine combustor (LSGTC)

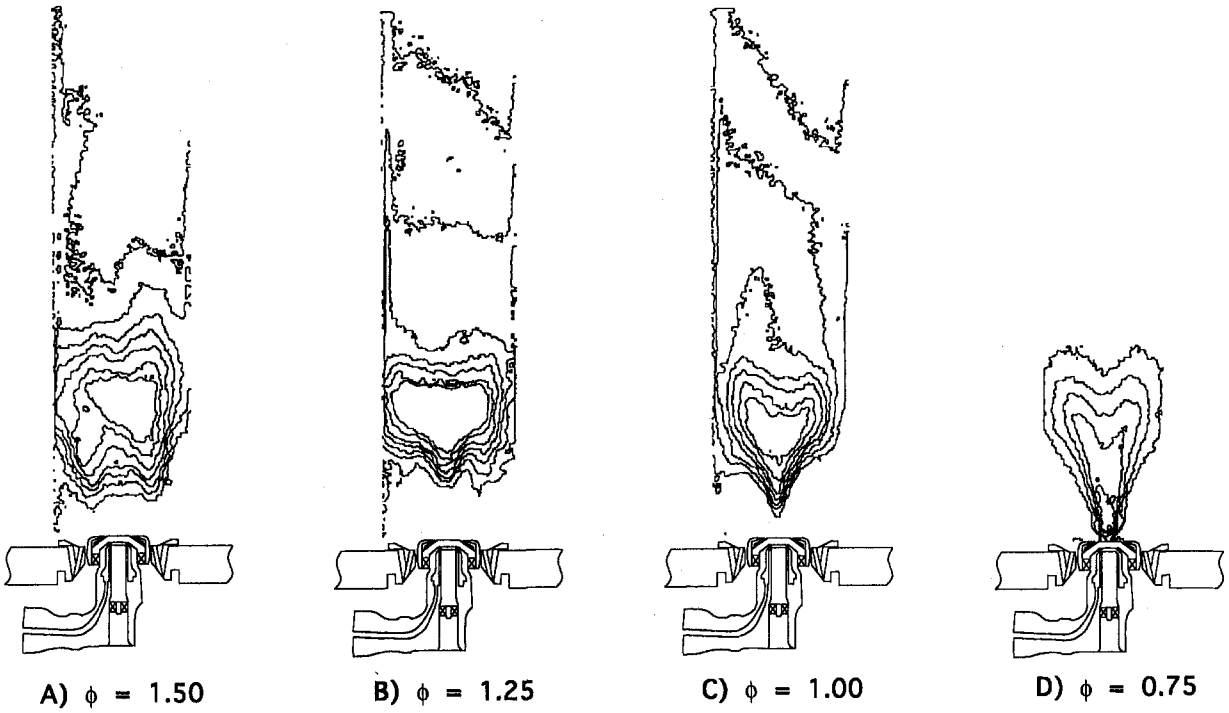

Fig. 3 Flame characteristics of the task 150-HS injector

Both mean gas velocity and mean gas temperature data were available for these two cases (ϕ = 0.75 and 1.50) from the earlier investigation (Hedman et al., 1994). Consequently, the differential mass balance, differential energy balance, pathline, and temperature timeline analyses were performed for these two specific cases and are discussed below.

Gas Velocity Measurements

LDA is a well-accepted diagnostic method for determining instantaneous gas velocity (e.g., Yeh and Cummins, 1964; Durst et al., 1976). Sample studies (Driscoll and Pelaccio, 1979; Zimmerman, 1985) are representative of the many investigations where velocity in combustion systems was determined using a LDA system.

A laser-Doppler anemometer (LDA) was used to make extensive measurements of mean and rms axial, radial, and tangential velocity data throughout the central part of the flame zone at two experimental conditions (500 slpm air flow rate, and ϕ = 0.72 and 1.49). These experimental data were reported in detail in the previous studies (Hedman et al., 1995; Hedman and Warren, 1994).

To obtain the local in situ data, the burner was translated along coordinate centerlines with respect to the laser diagnostic volume in X, Y, and Z coordinate directions. Translation in the X direction along the Y coordinate centerline allowed axial and radial velocity data to be obtained. The edge of the windows limited translation in this direction to about ±30 mm. Translation in the Y direction along the X coordinate centerline allowed axial and tangential velocity data to be obtained. As the diagnostic volume was brought near the quartz windows, significant optical noise was added to the Doppler signals. The quartz windows were approximately ±75 mm from the center of the reactor. The optical noise from the windows generally limited data collection to ±60 mm from the burner centerline.

Typically, data were collected at 0.5 or 1.0 mm radial increments where the velocity gradients were large. Data were collected at up to 10 mm increments where velocity profiles were relatively flat. A typical set of data was taken at axial locations of 10, 15, 20, 25, 50, 75, 100, 125, 150, 200, and 240 mm above the dome of the reactor. Occasionally, other intermediate locations were examined where large velocity gradients or other interesting behavior were found.

The radial and axial velocity data out to about ±30 mm from the centerline have been used in the differential mass and energy balance analysis, and in the pathline analysis. The mean radial and axial velocity data from the previous study (Hedman et al., 1995) for the two cases of interest (ϕ = 0.72 and 1.49) are summarized in Figs. 4 and 5. A more detailed discussion of the velocity results was made in the earlier paper. Figures 4 and 5 have been included in this paper to provide the reader with examples of the velocity results, and to provide an indication of the major flow features as evidenced by the isocontours of axial and radial velocity.

The LDA measurements shown in Figs. 4 and 5 are for the Task 150-HS burner. Mean radial and axial velocities are shown in Fig. 4 for lean conditions (ϕ = 0.72) where the flame was well attached to the central part of the injector, and in Fig. 5 for fuel-rich conditions (ϕ = 1.49) where the flame was attached to the dome and insert jets. Tangential velocity data do not affect either the differential mass or energy balances, and have not been shown herein. For the fuel lean case (ϕ = 0.72), the flame was fully attached to the center of the injector, and was relatively stable. The sharp peak in axial velocity component shown in Fig. 4 near the injector is clearly evident. The rapid decay of the high-velocity region near the injector as one moves downstream is also apparent. The recirculation zone directly over the injector is dramatic, and clearly shows a significant region of flow reversal. Recirculation patterns caused by the dome jets are not seen, but visual observations confirmed that recirculation in the corner between the dome and wall exists.

The radial velocity data are also presented in Fig. 4. These data are limited to a radial location of about 30 mm. The radial flow velocities are all very low in magnitude, but do show some interesting structures. The low magnitudes of these velocities are close to the resolution of the LDA instrument. A similar set of gas velocity data for the Task 150-HS combustor operating at a fuel equivalence ratio of 1.49 is presented in Fig. 5 for the mean axial and radial velocity measurements. The flame at this

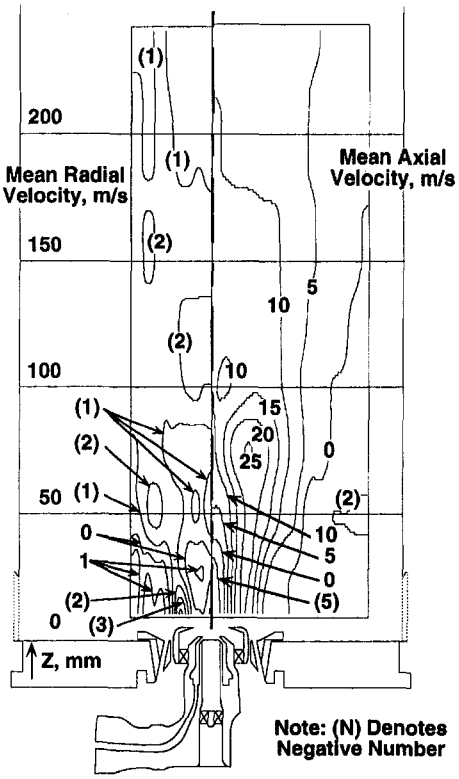

Fig. 4 Isovelocity contours at ϕ = 0.72 (T150-HS burner, 500 slpm air flow)

operating condition was attached to the insert and dome jets. As in Fig. 4, the radial data in Fig. 5 are limited to a radial location of about 30 mm, but the axial data in Fig. 5 were a composite of those collected along with both the radial (ca ± 30 mm) and the tangential (ca ± 60 mm) sets of data.

As for the ϕ = 0.72 case, the sharp peaks in mean axial velocity component associated with the injector are still clearly evident, but seem to decay more rapidly in the ϕ = 1.49 case. The recirculation zone directly over the injector is still dramatic, and shows little difference in the magnitude of the reversed velocity or in the size and shape of the recirculation pattern when compared to the ϕ = 0.72 case. The other major recirculation pattern in the combustor is of a similar shape to that observed with the ϕ = 0.72 case, but seems to be much stronger (i.e., has much larger reversed flow velocity components). The recirculation patterns caused by the dome jets are still absent. As with the ϕ = 0.72 case, visual observations confirmed that the corner recirculation still existed in this combustion flow case, but it was not possible to collect LDA close to the window near the bottom of the reactor because of optical noise near the quartz windows.

The radial velocity data for the ϕ = 1.49 case are also presented in Fig. 5. Again, the radial flow velocities are all very low in magnitude, but do show interesting structures that are quite different than seen with the lean flame. The low magnitudes of these velocities are also close to the resolution of the LDA instrument.

The differences in velocities between the lean flame and the rich flame show that there is a strong influence of the location of the flame zone on the flow fields as characterized by the measured velocity fields.

Lagrangian Pathline Analysis

Lagrangian pathlines were generated from the mean radial and axial velocity data by tracking fluid particles in the axial-radial flow field. The particles were introduced into the properly interpolated velocity data set at equally spaced positions along the sides and bottom of the flow field. Each particle's position was monitored as a function of time. Selected pathlines are presented in Figs. 6 and 7 for the ϕ = 0.72 and 1.49 cases of interest. The pathline analysis was only done for one-half of the combustor, doubled and reversed on the computer, and superimposed on the other side of the chamber.

These pathlines show two vortex centers and a stagnation point. The stagnation point occurs on centerline about 30 mm downstream of the injector. The vortex centers are associated with the recirculation zone just above the injector and the zone just outside the funnel shaped vortex. These pathlines give detailed information on the boundaries and intersections of the flow regions of the burner.

Comparing the pathlines for the two cases yields even subtler observations about the flow structure. The near injector region, in particular, shows significant differences. The stagnation point has moved slightly and the recirculation zones have changed accordingly in the fuel rich case (ϕ = 1.49, Fig. 7). Along the bottom, the flow between 15 and 30 mm is no longer axially positive, indicating a change in the outer recirculation zone. The small recirculation zone directly over the injector observed at ϕ = 0.75 (Fig. 6) is much smaller when ϕ = 1.50 (Fig. 7).

These Lagrangian pathlines mark representative reaction paths through the flame zone. As such, they have been used in a subsequent section to determine temperature time lines along representative paths in the base recirculation zone, in the mid or central recirculation zone just above the injector, and along a path leaving the injector and flowing directly out of the combustor for both the ϕ = 0.72 and 1.49 cases.

Gas Temperature Measurements

Eckbreth (1988) provides an excellent summary of CARS, a proven technique for determining gas temperature and limited

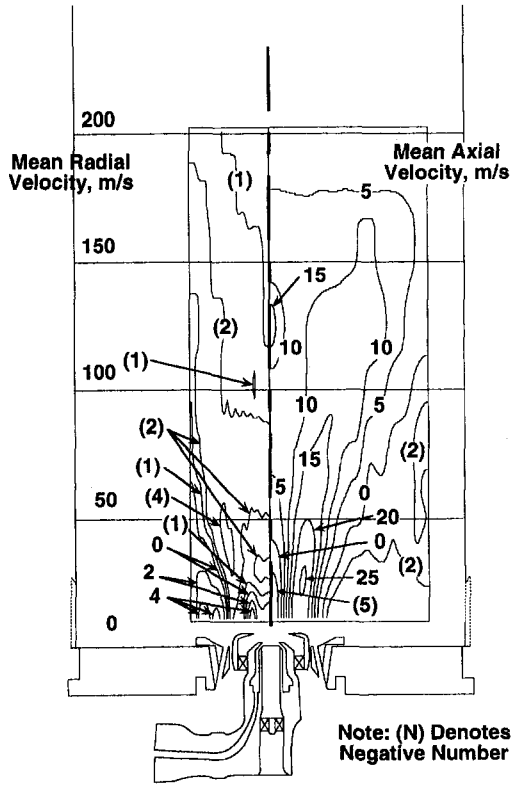

Fig. 5 Isovelocity contours at ϕ = 1.49 (T150-HS burner, 500 slpm air flow)

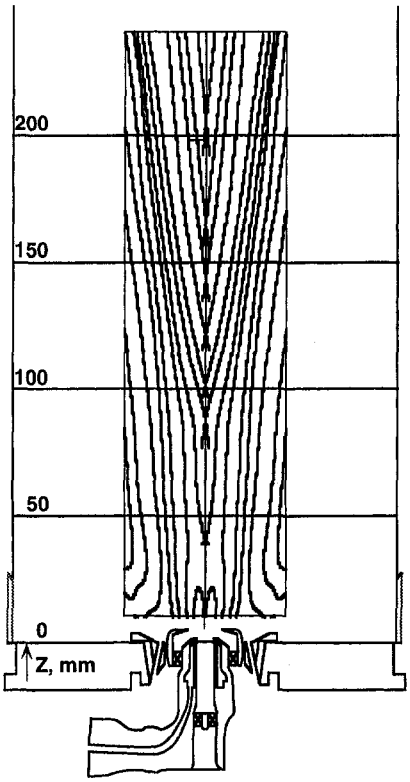

Fig. 6 Mean flow pathlines at ϕ = 0.72 (T150-HS burner, 500 slpm air flow)

species concentrations in turbulent combustion environments. Representative studies (Eckbreth et al., 1984, Greenhalg, 1987; Goss et al., 1988; Boyack and Hedman, 1990; Hancock et al., 1991; Zhu et al., 1993) provide examples of the broad application of CARS to obtain temperature and/or species concentration in combustion environments. The BYU CARS instrument has been described in detail elsewhere (Boyack and Hedman, 1990; Hancock et al., 1991).

Coherent anti-Stokes Raman spectroscopy (CARS) was used to obtain a set of gas temperature measurements in the Task 150-HS combustor at ϕ = 0.75, 1.00, 1.25, and 1.50; and at an air flow rate of 500 slpm (Hedman et al., 1994). Like the gas velocity measurements, the CARS temperature measurements were taken at closely spaced radial increments where large gradients in temperature were found and in a courser grid where the temperature gradients were relatively shallow. Temperature data were taken at similar axial locations as well. The temperature data were taken along the X coordinate, and consequently are available only out to a radius of about 30 mm, but were taken to an axial location of about 300 mm.

Figure 8 and 9 present isocontour plots of mean temperature data for the Task 150-HS combustor operating with an air flow rate of 500 slpm and at fuel equivalence ratios of 0.75 and 1.50, the two cases of interest in this paper. The isocontour plots were duplicated, flipped, and added to the opposite side of the combustor to give a better representation of the temperature field in the vicinity of the injector.

The relatively cold region (600 K to 1000 K) directly above the injector in both cases generally corresponds the central recirculation zone seen in the gas velocity plots (Figs. 4 and 5). Surrounding the cold central zone is an intermediate temperature region that seems to be associated with the penetration of the very high axial velocity into the combustor. Higher temperatures exist on either side of this penetration zone. It is unfortunate that temperature data could not be obtained in the lower corners of the combustor where the recirculation zones near the dome are located. The data do suggest that this region is relatively cool for the ϕ = 0.75 case, but seem to indicate a relatively hot region in this corner recirculation zone for the ϕ = 1.5 case. This observation seems to be consistent with the observed relocation of the flame zone from the central core of the vortex when operating fuel-lean to the outer recirculation zone when operating fuel-rich.

For the ϕ = 0.75 case, the peak temperature measured was 2085 K, which is about 178 K below the theoretical stoichiometric (ϕ = 1.00) adiabatic flame temperature of 2263 K. The peak temperature (1875 K) in the fuel-rich case is about 99 K below the predicted adiabatic flame temperature of 1974 K for ϕ = 1.50.

Differential Control Volume Analysis

With both mean temperature and mean velocity data sets available at identical flow conditions, it became possible to combine the information to extract information unmeasurable by other means, which gives further insights into the combustion processes. To accomplish this analysis, it was necessary to adapt numerical methods normally employed for theoretical modeling to extract these additional observations (differential mass and energy balances, and temperature timelines through the flame from the Lagrangian pathline analysis) from the experimental results.

This study made use of differential control volumes, commonly used in thermal and fluid sciences, to determine the local mass and energy balance throughout the flame zone. The shape of a control volume is arbitrary but is always bounded by a closed control surface. For this analysis, the cylindrical steady-state finite difference control volumes illustrated in Fig. 10 were used. Each cylindrical control volume has four distinct sides across which mass and energy transfer. The region over which data were collected was divided into control volumes 1 mm wide and 2 mm high rotated about the centerline. Since a region

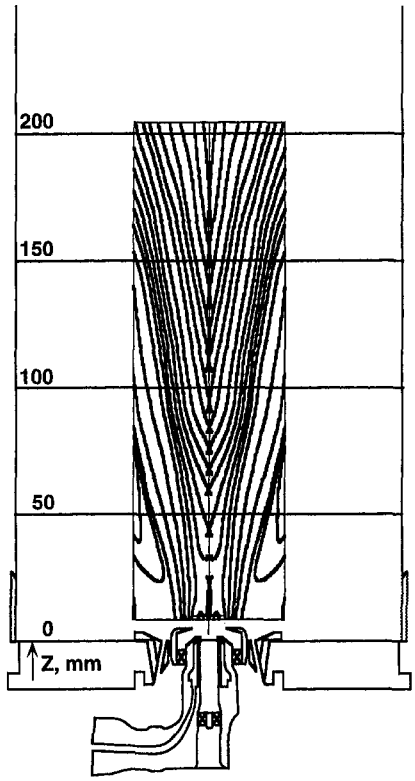

Fig. 7 Mean flow pathlines at ϕ = 1.49 (T150-HS burner, 500 slpm air flow)

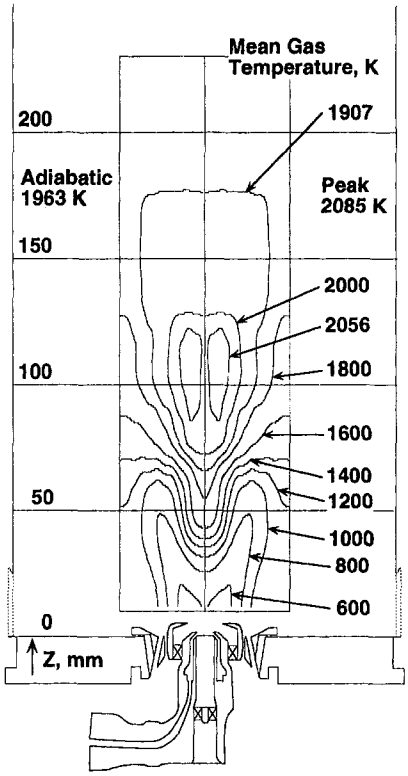

Fig. 8 Isotemperature contours at ϕ = 0.75 (T150-HS burner, 500 slpm air flow)

of about 30 mm from the centerline and from 10 mm to 200–240 mm in axial coordinate was analyzed, about 2850 to 3450 separate cylindrical control volumes were considered in the

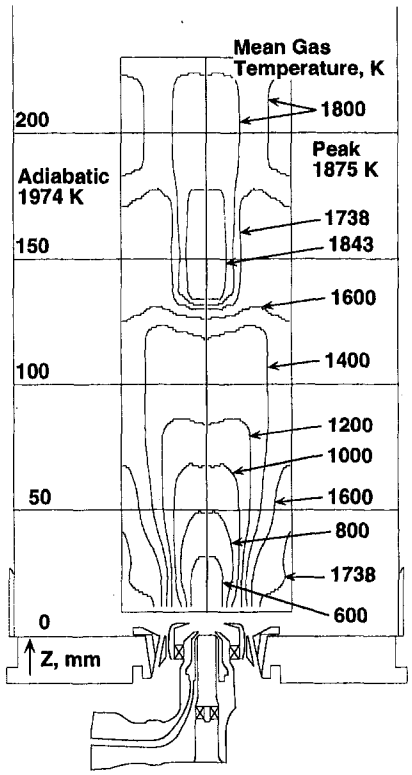

Fig. 9 Isotemperature contours at ϕ = 1.50 (T150-HS burner, 500 slpm air flow)

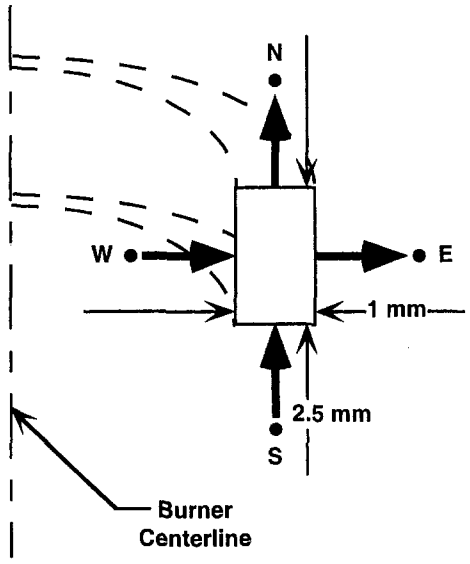

Fig. 10 Differential two-dimensional axisymmetric control volume

flame zone. Suitable interpolation of the velocity and temperature data provided the velocities and temperatures at the boundaries of each of the control volumes to be determined.

The first check done on the control volumes was to check the mass storage term. Being at steady state, the mass entering the control volume should be balanced by the mass leaving the control volume. The mass crossing any given side of the control surface was calculated from

$$\dot{m} = \rho V A \tag{1}$$

where

$\dot{m}$ is the mass flux,
ρ is the gas density,
V is the velocity perpendicular to the control surface,
and A is the area of the side.

Some estimate of the density must be made to use this equation. Density is a function of temperature, pressure, and gas composition. Pressure and composition were not measured in this study and therefore were approximated. The pressure was assumed to be constant at 1 atm. All properties that depended upon composition were calculated assuming the physical properties of air. Although temperature data were interpolated to obtain control volume temperatures, the temperature used in the density calculation was based on an upwind scheme. In this scheme, if the vertical velocity carried mass from the control volume labeled S (south) into the P control volume, the mass flux is considered to have the properties associated with the characteristics of the S control volume. By applying these assumptions to each side of the control volumes, estimates for the mass fluxes were obtained. These results were used to calculate an estimated conservation of mass error for each control volume in the combustor using Eq. (2). This local error provides an estimate on the quality of data, and indicates regions where high quality data are difficult to obtain.

$$\text{percent error} = \frac{\text{mass}_{\text{in}} - \text{mass}_{\text{out}}}{\text{mass}_{\text{in}}} \times 100 \text{ percent} \tag{2}$$

Images of the local "conservation of mass" error are presented in Figs. 11 and 12 for ϕ = 0.75 and 1.50, respectively. In general, the error in local mass balance was less than ±10 percent. There were exceptions in regions of the burner where the local error exceeded ±20 percent for the ϕ = 0.75 case, and ±50 percent for the ϕ = 1.50 case. These areas were in

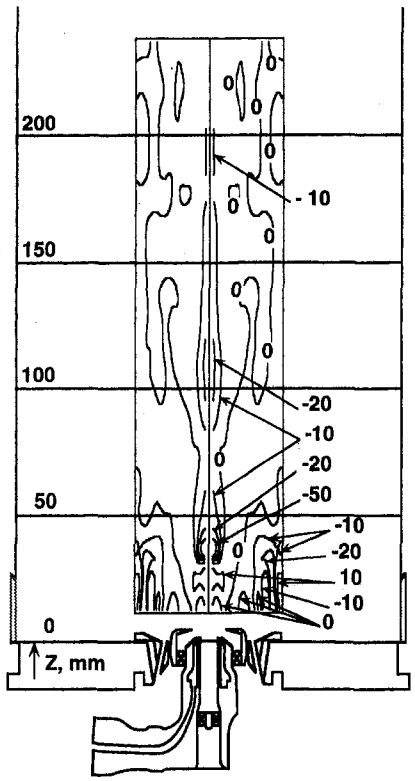

Fig. 11 Differential mass balance (percent) at $\phi = 0.75$ (T150-HS burner, 500 slpm air flow)

the high shear areas associated with the insert jets, or the strong recirculation zone on the centerline just above the injector.

Calculation of the enthalpies and kinetic energies associated with each mass flow was a relatively simple process. Initial efforts for the energy balance, however, were met with failure. The amount of energy being transported through each control volume is much greater than the amount being released. Thus, even small errors in mass balance cause severe numerical noise. A simpler, more robust scheme was developed that forced the mass balance before doing the energy calculations.

The simplified scheme calculated the heat release in a given control volume using:

$$H_r = \dot{m} \times (h_{\text{in}} - h_{\text{out}}) \tag{3}$$

where:

H_r is the energy release
$\dot{m}$ is the net mass flux into the volume.
h_{in} is the net enthalpy of the gas entering the volume
h_{out} is the net enthalpy of the gas leaving the volume

The incoming thermal energy is associated with the incoming mass and its enthalpy; the outgoing energy calculation was done with the mass entering the control volume and the characteristics of the control volume (as per the upwind scheme). This scheme has the significant advantage of not losing mass and its associated energy while lacking only the capability of calculating the kinetic energy (due to the unknown outgoing velocities). In the relatively low velocity flows in this study, kinetic energy (~0.2 kJ/kg) was negligible in comparison to the thermal energy (150 kJ/kg) being released by the combustion processes, and was neglected in the energy balances performed.

The calculated heat release has been reported as the total heat release in the differential control volume per unit time normalized by the differential volume. Images mapping the heat release per unit volume are presented in Figs. 13 and 14 (ϕ = 0.75 and ϕ = 1.50, respectively) and can be compared to the isochromatic video images (Fig. 3(*D*) and 3(*A*)) for the same test conditions. Figure 13 is remarkable in its similarity to the visible flame. The fuel-rich case (ϕ = 1.5) reveals a band of energy release about 125 mm downstream. This extra energy release is likely the result of the hot, fuel-laden combustion products encountering more oxygen, most likely from the dome jets. This region of higher energy release generally corresponds to the visual flame structure (Fig. 3(*A*)). In general, the flame structure at the fuel-rich condition (ϕ = 1.5) is not as coherent as the structure observed for the lean condition. This is evident in both the energy release contour plots and in the digitized video images.

An integration of the energy released was also done over the entire computational domain. The computational domain was limited by the optical access into the burner and did not include the entire combustion zone. The result of the integrations, along with the chemical energy being introduced into the burner, is summarized in Table 1. There are some factors that are not considered. Radiation heat losses and heat release, which take place outside the computational field of view, were not considered. Also, the chemical energy that left the combustor as unburned fuel was not included.

Table 1 reports the amount of thermal energy being released and the chemical energy being released. The thermal energy being released does not include any corrections for radiation losses nor does it include any energy released outside the computational range.

At ϕ = 0.75, almost 79 percent of the energy introduced into the burner is released in the computational flame zone analyzed. However, at ϕ = 1.50, only about 21.5 percent of the energy introduced into the burner as fuel is released in this zone. The large discrepancy in the fuel-rich case is thought to be primarily due to heat release outside the computational field (e.g., in the corner recirculation zone) and chemical energy leaving the system as unreacted fuel.

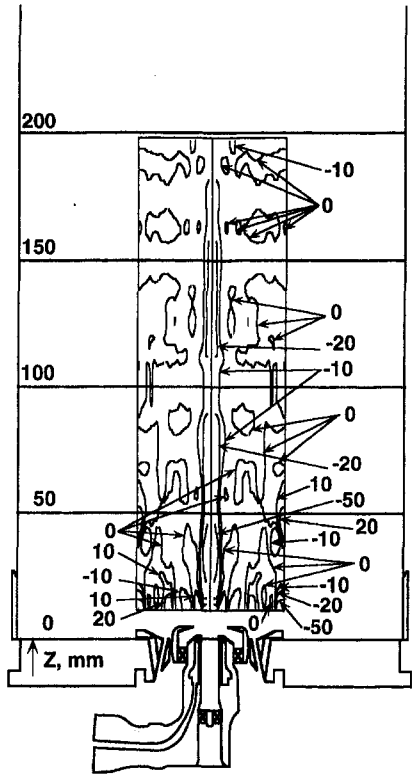

Fig. 12 Differential mass balance (percent) at $\phi = 1.50$ (T150-HS burner, 500 slpm air flow)

Temperature Timelines

The local velocity and temperature data were combined with the Lagrangian pathline analysis in an attempt to gain some additional insights about the reactions rates associated with the combustion of the propane fuel. In this analysis, the combination of velocity data along a pathline allowed the time as a function of position to be easily determined. The convolution of this time and position with the known local temperature allowed temperature timelines along the Lagrangian pathline to be determined. As the fluid particle traces out the pathline, both the elapsed time and the particle's position are known.

By referencing the particle's position to the temperature field, a temperature versus time plot was obtained for that fluid particle. Examples of the temperature timelines for selected pathlines are presented in Figs. 15 and 16 for the ϕ = 0.75 and 1.50 cases, respectively. Temperature timelines on pathlines leaving the injector, in the base recirculation zone, and in the midrecirculation region are shown.

The timeline plots give considerable insight about the combustion rate of the propane fuel. The timeline data presented include the effects associated with the turbulent mixing of the fuel and air in the diffusion burner, and the chemical kinetics of the complex reaction mechanisms associated with the oxidization of propane. In the fuel lean case, Fig. 15, the three curves (injector, midrecirculation, and base recirculation) are very similar. Each curve has an almost identical slope. The similar slopes indicate that each fluid particle experienced similar combustion rates. The particles in the midrecirculation zone also lost energy (i.e., lower temperature) before entering a reaction zone. These decreases were likely due to the mixing of more fuel and air mixture from the injector. This conclusion is supported in the base recirculation zone, which lost even more temperature in the mixing prior to reaction, but also gained more temperature during combustion. This figure implies the primary combustion zone lies on the boundary of the injector flow and the outside recirculation zone.

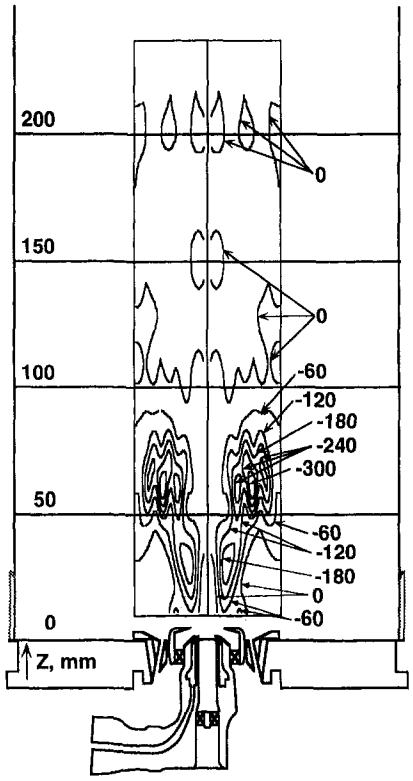

Fig. 13 Energy release (kJ/m^3·s) at ϕ = 0.75 (T150-HS burner, 500 slpm air flow)

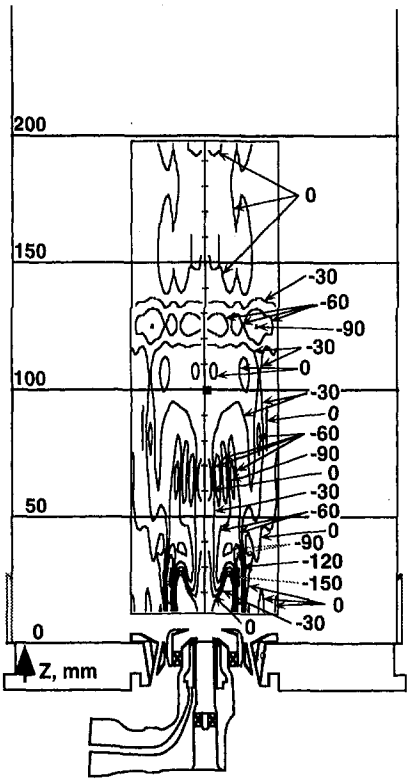

Fig. 14 Energy release (kJ/m^3·s) at ϕ = 1.50 (T150-HS burner, 500 slpm air flow)

In the fuel-rich case, Fig. 16, only the particle that started near the injector underwent a large temperature change. These particles began with a temperature higher than the temperature of the reactants being introduced into the chamber through the injector. This high temperature was slightly cooled before entering the combustion zone, indicating the injected gases mixed with the hot recirculation products prior to mixing with the injector combustor air stream.

Comparing Figs. 15 and 16 with the corresponding CARS temperature figures (Figs. 8 and 9) confirms the same trends observed in the CARS data, namely, the recirculation zone when ϕ = 1.50 was much hotter than when ϕ = 0.75. The rate of temperature rise was nearly double (300,000–400,000 K/s) for the lean case than for the fuel-rich (ca 150,000 K/s) suggesting either a slower diffusion process or again, a slower combustion process for the richer case.

Observations and Conclusions

This study has contributed to an improved understanding of the operational characteristics of a practical injector. However, much more needs to be done before a full understanding of the combustion characteristics of a practical gas turbine combustor is achieved.

The location of the flame fronts, the flame shape, and the stability of the flame were found to be a strong function of the fuel equivalence ratio. The different flame structures arose from changes in the flow fields and mixing patterns as fuel equivalence ratio was varied. The flames were attached to the insert air jets when the burner was operated very fuel-rich, but would lift, reattach, and lift again as the fuel equivalence ratio was progressively reduced. When attached to the burner, the flame took on the characteristics of a strong vortex flow. Two different flame structures were the subject of this analysis, one where the flame was well attached to the injector (ϕ = 0.72), and one at fuel-rich conditions (ϕ = 1.49) where the flame was attached to the dome and insert jets.

Table 1 Energies associated with the task 150-HS burner

Phi	Thermal Energy Released (kW)	Chemical Energy Introduced (kW)
0.75	16.3	20.7
1.50	8.9	41.4

Gas velocity measurements were made with an LDA at both the fuel-lean ($\phi = 0.72$) and fuel-rich conditions ($\phi = 1.49$). Gas velocity data near the injector have shown sharp peaks in mean axial velocity near the outlet of the injector, and a corresponding strong tangential component in this same location. The insert jets had a marked influence on the axial and radial components. The sharp gradients in axial and tangential velocity components decayed rapidly, becoming nearly uniform across the duct by the 150 mm axial location.

CARS gas temperature measurements were also made in the Task 150-HS combustor. The variation in temperature field as the fuel equivalence ratio changes from fuel-lean to fuel-rich was consistent with the observations made from the digitized video images. In general, the temperature measurements were consistent with visual flame observations, PLIF images of the OH radical, and velocity measurements.

A differential control volume analysis was used to compute mass and energy balances on 1 mm by 2 mm cylindrical control volumes throughout the computational flame zone. The mass balance showed modest errors through most of the flame (ca $\pm$ 10 percent) except near regions of high shear and mixing (insert jets and central recirculation zone) where differential mass balance errors of about $\pm$20 percent were seen for the fuel lean case, and $\pm$50 percent for the fuel rich case.

The differential energy balance analysis showed the regions of high energy release very well, and provided quantitative values for the rate of energy release in the flame zone (up to ca 400 kJ/m^3·s at $\phi = 0.75$ and ca 200 kJ/m^3·s at $\phi = 0.75$). This technique worked best when the flame consumed nearly all chemical energy available within the computational field of view.

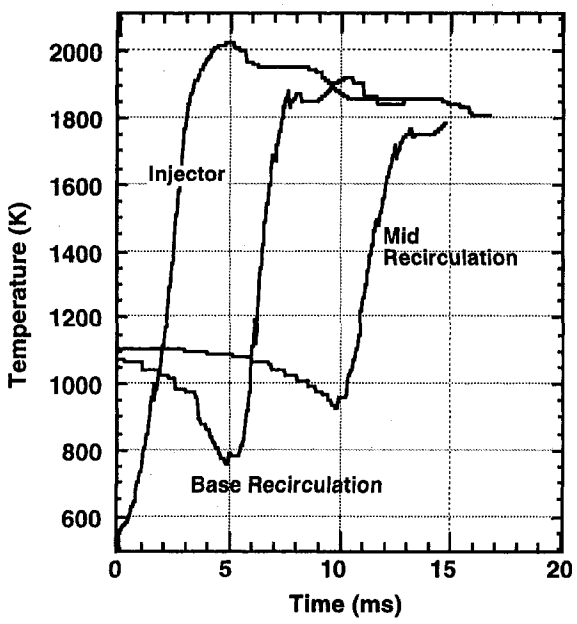

Fig. 15 Temperature–time histories along selected pathlines through the flame zone (500 slpm air flow, $\phi = 0.75$)

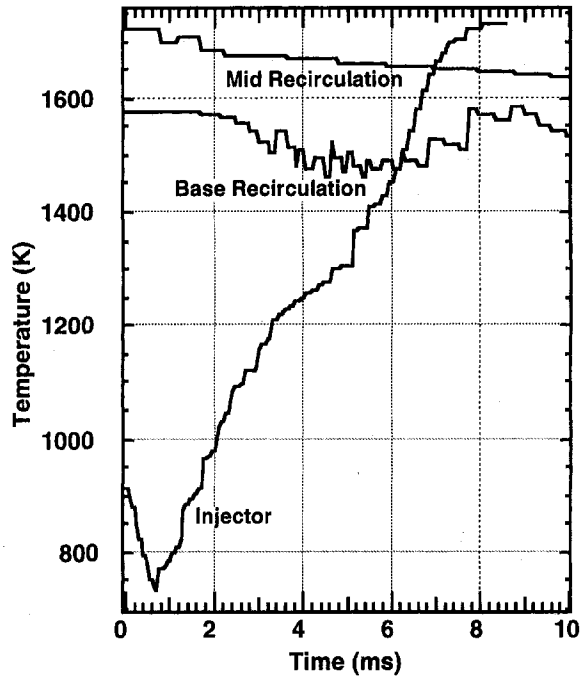

Fig. 16 Temperature–time histories along selected pathlines through the flame zone (500 slpm air flow, $\phi = 1.5$)

The local mean axial and radial velocity data were appropriately interpolated, and used to determine Lagrangian pathlines throughout the computational flame zone. These pathlines indicate regions of recirculation and stagnation points. They also provide a convenient locus of gas particles through the flame zone, which can be used to track path dependent combustion phenomena. These pathlines along with the local velocity and temperature were used to deduce temperature timelines throughout the computational flame zone. These temperature timelines show that complete combustion of propane, including mixing and chemical reaction rate effects, takes from 5 to 10 ms to occur depending on path and overall stoichiometry. The analysis also shows temperature rise rates of about 150,000 K/s for the fuel-rich ($\phi = 1.50$) case, and about 300,000–400,000 K/s for the fuel-lean ($\phi = 1.50$) case.

Acknowledgments

This paper presents results from an Air Force Office of Scientific Research (AFOSR) program being conducted at Brigham Young University (BYU), Provo, Utah, and at Wright-Patterson Air Force Base (WPAFB). This study is part of an extensive research effort being carried out by the Fuels Combustion Group of the Aero Propulsion and Power Laboratory at Wright-Patterson Air Force Base (APPL, WPAFB), Dayton, Ohio, in which simple and complex diffusion flames are being studied to better understand the fundamentals of gas turbine combustion. The program's long-term goal is to improve the design methodology of gas turbine combustors.

References

Boyack, K. W., and Hedman, P. O., 1990, "Dual-Stokes CARS System for Simultaneous Measurement of Temperature and Multiple Species in Turbulent Flames," *Twenty-Third Symposium (International) on Combustion,* The Combustion Institute, Pittsburgh, PA, pp. 1893–1899.

Driscoll, J. F., and Pelaccio, D. G., 1979, "Laser Velocimetry Measurements in a Gas Turbine Research Combustor," *Laser Velocimetry and Particle Sizing,* Proc. Third International Workshop on Laser Velocimetry, D. H. Thompson and W. H. Stevenson, eds., Hemisphere publishing Co., Washington, DC.

Durst, F. A., Melling, A., and Whitelaw, J. H., 1976, *Principles and Practice of Laser Anemometry,* 1st ed., Academic Press, London.

Eckbreth, A. C., 1988, *Laser Diagnostics for Combustion Temperature and Species,* Abacus Press, Cambridge, MA.

Eckbreth, A. C., Dobbs, G. M., Stufflebeam, J. H., and Tellex, P. A., 1984, "CARS Temperature and Species Measurements in Augmented Jet Engine Exhausts," *Applied Optics,* Vol. 23, pp. 1328–1339.

Goss, L. P., Trump, D. D., and Roquemore, W. M., 1988, "Combined CARS/LDA Instrument for Simultaneous Temperature and Velocity Measurements," *Experiments in Fluids,* Vol. 6, Springer-Verlag, pp. 189–198.

Greenhalg, D. A., 1987, "Quantitative CARS Spectroscopy," *Advances in Non-linear Spectroscopy,* Chap. V, R. J. H. Clark and R. E. Hester, eds., Wiley, New York.

Hancock, R. D., Hedman, P. O., and Kramer, S. K., 1991, "Coherent Anti-Stokes Raman Spectroscopy (CARS) Temperature and Species Concentration Measurements in Coal-Seeded Flames," *Combustion and Flame,* Vol. 71, pp. 593–604.

Hedman, P. O., and Warren, D. L., 1994, "Turbulent Velocity and Temperature Measurements From a Gas-Fueled Technology Combustor with a Practical Fuel Injector," Paper No. 25-705, The Twenty-Fifth International Symposium on Combustion, The University of California at Irvine, Irvine, CA.

Hedman, P. O., Sturgess, G. J., Warren, D. L., Goss, L. P., and Shouse, D. T., 1995, "Observations of Flame Behavior From a Practical Fuel Injector Using Gaseous Fuel in a Technology Combustor," ASME JOURNAL OF ENGINEERING FOR GAS TURBINES AND POWER, Vol. 117, pp. 441–452.

Sturgess, G. J., Sloan, D. G., Lesmerises, A. L., Heneghan, S. P., and Ballal, D. R., 1992, "Design and Development of a Research Combustor for Lean Blowout Studies," ASME JOURNAL OF ENGINEERING FOR GAS TURBINES AND POWER, Vol. 114, pp. 13–19.

Yeh, Y., and Cummins, H. Z., 1964, "Localized Fluid Flow Measurements With an He–Ne Laser Spectrometer," *Applied Physics Letters* Vol. 4, pp. 176–178.

Zhu, J. Y., Tsuruda, T., Sowa, W. A., and Samuelsen, G. S., 1993, "Coherent Anti-Stokes Raman Scattering (CARS) Thermonetry in a Model Gas Turbine Can Combustor," ASME JOURNAL OF ENGINEERING FOR GAS TURBINES AND POWER, Vol. 115, pp. 515–521.

Zimmerman, D. R., 1985, "Laser Anemometer Measurements of the Flow From a Simulated Fuel Nozzle," *International Symposium on Laser Anemometry,* A. Dybbs and P. A. Pfund, eds., Winter Annual Meeting of ASME, FL.